On the pump mode shutdown sequence for a model contra-rotating pump-turbine

Citation for the original published paper (version of record):
Fahlbeck, J., Nilsson, H., Salehi, S. (2025). On the pump mode shutdown sequence for a model contra-rotating pump-turbine. IOP Conference Series: Earth and Environmental Science, 1483(1).
http://dx.doi.org/10.1088/1755-1315/1483/1/012016

IOP Conference Series:
Earth and
Environmental Science

PURPOSE-LED PUBLISHING™

PAPER • **OPEN ACCESS**

On the pump mode shutdown sequence for a model contra-rotating pump-turbine

To cite this article: J Fahlbeck *et al* 2025 *IOP Conf. Ser.: Earth Environ. Sci.* **1483** 012016

On the pump mode shutdown sequence for a model contra-rotating pump-turbine

J Fahlbeck, H Nilsson and S Salehi

Department of Mechanics and Maritime Sciences, Chalmers University of Technology, SE-412 96 Gothenburg, Sweden

E-mail: `fahlbeck@chalmers.se`

Abstract. Contra-rotating pump-turbines are currently being studied in the ALPHEUS EU H2020 project as an alternative for low-head pumped hydro storage (PHS). To have an efficient PHS facility, it is important to know how to operate the pump-turbine unit under transient conditions to be able to adapt to demand variations rapidly. Therefore, this study focuses on the transient pump mode shutdown sequence of a contra-rotating pump-turbine. Two different sequences are evaluated using computational fluid dynamics simulations. The sequences are denoted as 'preliminary' and 'new' since the preliminary sequence is similar to a sequence in one of our earlier studies. It is shown that the preliminary sequence produces reverse flow and large load gradients on the runners. The new sequence manages to avoid reverse flow and reduces the load gradients. The main reason the new sequence is advantageous is because a valve is closed before speeding down the runners. However, the new sequence produces larger load fluctuations, and a wider frequency spectrum of pressure fluctuations, compared to the preliminary sequence.

1. Introduction

Low-head pumped hydro storage (PHS) is one solution to aid the growing need for energy storage because of the increasing share of intermittent renewable energy sources [1]. Low-head PHS is generally relevant in countries that lack high mountain regions where it is not possible to construct typical high-head PHS. New runner designs with contra-rotating pump-turbines (CRPT) have been suggested as an alternative configuration for low-head PHS [2]. The ALPHEUS (Augmenting Grid Stability Through Low Head Pumped Hydro Energy Utilization and Storage) EU H2020 [3] project has the aim to study CRPTs for low-head PHS.

Preliminary studies of the CPRT pump mode startup and shutdown sequences [4] have shown that the runners may be subjected to large and rapid load variations. Large load variations can potentially damage the machine after enough cycles. It is for that reason important to study transient sequences to understand how the potentially detrimental load variations can be limited. The pump mode startup sequence of the CRPT has recently been comprehensively analysed and optimised by Fahlbeck et al. [5, 6]. However, the CRPT pump mode shutdown sequence has until the present day not gained much attention. The current study is for that reason investigating two alternative shutdown sequences with the help of computational fluid dynamics (CFD) simulations. One of the evaluated sequences is based on our earlier work [4] and is denoted 'preliminary', and the other sequence is denoted 'new' since it has not been examined previously.

The studied model scale CRPT and its mounting arrangement, together with a schematic of the shaft alignment, is depicted in Fig. 1a. A model scale geometry is used in this study because the machine is later to be experimentally tested as a part of the ALPHEUS project to validate the CFD simulations. The illustrated mounting arrangement is only for the model scale. In the prototype scale another type of mounting is to be expected, as discussed by Truijen et al. [7]. For the current CRPT, Runner 1 is located upstream and Runner 2 is placed downstream in pump mode. Each runner is connected to an individual motor/generator unit via the shafts that go inside the hub and one of the support struts, through a bevel gear. The runner rotational speeds can thus be controlled individually.

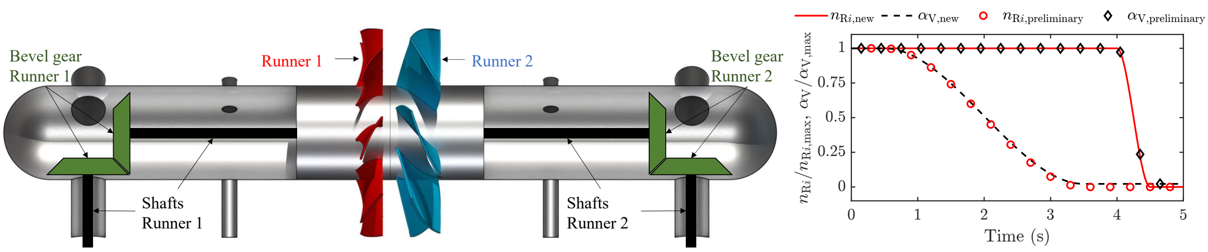

(a) (b)

Figure 1. Pump-turbine geometry and mounting arrangement (a), and normalised shutdown sequences (b). The preliminary sequence in (b) is equivalent to that of Fahlbeck et al. [4].

2. Method

The evaluated shutdown sequences are shown in Fig. 1b. The sequences start with a fully developed flow field at a fixed operating condition. At the initial conditions, the machine consumes 23.8 kW, produces a net head of 7.9 m and a flow rate of 270 l/s. The resulting hydraulic efficiency of the machine is about 87%. Furthermore, the initial rotational speed of Runner 1 is 1129.1 rpm ($n_{\mathrm{R1,max}}$), and Runner 2 rotates at 848.9 rpm ($n_{\mathrm{R2,max}}$). During the shutdown, the rotational speed of the runners ($n_{\mathrm{R}i}$) is reduced simultaneously, and a valve (α_{V}) is closed. The curves in Fig. 1b indicate the new, previously not investigated sequence, while the markers display the preliminary sequence. In the new sequence, the valve is first closed between 0.5–3.5 s. This is followed by the speed-down of the runners between 4–4.5 s. On the other hand in the preliminary sequence, the valve closure and runners' speed-down are in the opposite of the new sequence. This means that in the preliminary sequence, the runners' speed-down occurs within 0.5–3.5 s, followed by the closing of the valve between 4–4.5 s. After the shutdown an addition of half a second is simulated to show stable conditions subsequent to the sequences.

2.1. Numerical set-up

The incompressible Reynolds averaged Navier-Stokes equations are discretised and solved on a computational mesh with the OpenFOAM-v2112 open-source CFD code. For closure and to account for turbulence, the k-ω SST-SAS [8] (shear stress transport - scale adaptive simulation) model is used. Several recent studies have provided confidence that the turbulence model can accurately predict the flow field for a hydro turbine [9, 10].

The second-order accurate linear upwind stabilise transport (LUST) scheme [11] is used to discretise the convection terms of the three momentum equations. The first-order accurate upwind scheme is applied to the convection terms of the turbulent quantities k and ω. All other terms are discretised with the second-order accurate central difference scheme. Time derivatives are taken care of by the second-order backward scheme [12]. A constant time step of 5×10^{-5} s is used, equivalent to a maximum runner rotation of 0.34° per time step.

IOP Conf. Series: Earth and Environmental Science **1483** (2025) 012016 doi:10.1088/1755-1315/1483/1/012016

The mesh is divided into four parts, one for each of the runners, and the two domains that are located before and after the CRPT. The arbitrary mesh interface [13] technique is used to transfer fluxes at the sliding interfaces that connect the mesh regions. The total cell count of the numerical domain is around 12×10^6 cells. Each of the runner regions has about 2×10^6 cells, and the two parts up and downstream consist of around 4×10^6 cells each. The maximum y^+ is 114, and the y^+ is below 37 in 99% of the computational domain. Wall functions with all y^+ treatments are thus employed.

The `headLossPressure` boundary condition [14] is used at the inlet and outlet of the numerical domain to achieve flow-driving pressure differences. The boundary condition is configured to account for the components that are not part of the numerical domain by prescribing head losses in accordance with a future lab test facility. The valve sequence through the pump shutdown is controlled as a time-varying head loss at the outlet boundary since the valve is located downstream of the CRPT. The input data for the `headLossPressure` boundary condition is the same as in Table 2 in reference [6] (not shown here, for brevity).

3. Results and discussion

The main interest in the present study of the CRPT machine is to understand how the flow rate and loads change during the shutdown sequence. For that reason, Fig. 2 shows the computed flow rate (left), and integrated axial force (middle) and torque (right) on the runner blade surfaces through the shutdown sequences. The instantaneous average loads are displayed as solid curves and the shaded curves are the instantaneous loads.

The computed flow rate, left in Fig. 2, reveals distinct differences between the two sequences. In the new sequence the change of flow rate is smooth as the valve is closing, and a near zero flow is seen by the time of 3.1 s. However, in the preliminary sequence the flow rate is rapidly decreasing as the rotational speed of the runners is reduced. At 1.9 s, a zero-flow rate is encountered and after that time the flow rate accelerates in the reverse direction. As the runners are at a standstill and the valve is fully open, between 3.5–4 s, a reverse flow of around 0.15 m^3/s is experienced. As the valve is closing the reverse flow is reduced to zero.

The runner loads, axial force and torque are shown in the middle and right graphs of Fig. 2, respectively. As for the flow rate, the loads show clear differences between the two sequences. For instance, the new sequence shows an almost constant load variation up until 2 s. At that time the Runner 2 loads indicate a smooth increase. The peak Runner 2 loads occur at 2.5 s, and at this point the runner is exposed to an axial force of 2.5 kN and a torque of 140 N·m. After the Runner 2 peak, the loads rapidly reduce and reach a plateau at 3.2 s. At that time the valve is almost completely closed and the load fluctuations are enlarged. The Runner 1 axial force is starting to increase after 2 s in the new sequence. Later in the sequence the axial force decreases between 2.5–2.8 s, and thereafter a plateau is reached. The torque is on

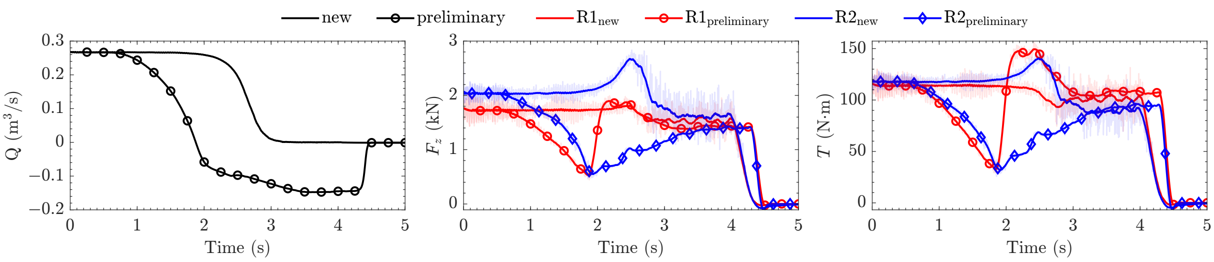

Figure 2. Computed flow rate Q, runner axial force F_z, and runner torque T, during the shutdown sequences. The solid load curves show the instantaneous average value of the signal and the shaded curves show the instantaneous signal.

the other hand only slowly decreasing up until 2.8 s. Also for Runner 1, the load fluctuations increase as the plateau is reached. Later, as the runners are brought to a standstill, the loads follow the decreasing rotational speed, ending up with a zero-load condition as the shutdown is finished. In the preliminary sequence the loads reduce as the rotational speed of the runners starts to decrease. Initially the loads follow the decreasing rotational speed. However, at the time of zero flow rate at 1.9 s, the smooth change in load variation is drastically interrupted. The Runner 1 loads make a sudden jump and the torque is increased by a factor of 4.6 during a very short period of time, as the flow rate accelerates in the reverse direction. The Runner 2 loads do not show this drastic change. It is only gradually increasing as the runners are brought to a standstill. During the valve closure the runner loads reduce to zero as the reverse flow is diminished because of the closing valve.

The larger load gradients encountered in the preliminary sequence, compared to the new sequence, are presumably not desirable. This is because large and rapid load variations can harm the safety and lifetime of the machine because of low-frequency fatigue. In one of our earlier studies [6] the CRPT pump mode startup sequence was optimised with the objective function

$$f = \int \left(\left| \frac{\partial \bar{F}_{z,\mathrm{R1}}}{\partial t} \right| + \left| \frac{\partial \bar{F}_{z,\mathrm{R2}}}{\partial t} \right| \right) \mathrm{d}t,$$

where the force is the instantaneous average in kN. By computing the corresponding objective function in the new and preliminary sequences it is found that the new sequence produces a smaller value and should thus be a preferable option. The new sequence achieves a value of 9.5 kg·m/s^2, while the preliminary reaches a value of 10.6 kg·m/s^2, which is about 11% larger.

Figure 3 shows flow structures at three time steps during the shutdown sequences, with the new sequence to the left and the preliminary sequence to the right. At time 1.5 s in the new sequence (Fig. 3a) the machine is essentially at the initial operating condition since the flow rate is still at 100%. Leading edge tip vortices are noted for both runners and some trailing edge flow structures are demonstrated. At the same time in the preliminary sequence (Fig. 3b) the flow rate is down at 57% of the initial flow rate. The flow structures around the runners are less organised compared to the new sequence. Later on, at 2.5 s, the flow structures in the new sequence (Fig. 3c) are breaking up because of the decreasing flow rate. In the preliminary sequence (Fig. 3d), reverse flow is experienced and the flow structures are starting to develop in the reverse direction. At the time of 3.5 s, the valve is fully closed in the new sequence (Fig. 3e) while the runners are rotating at their initial speeds. Large flow structures are formed between the runners, which causes the larger load fluctuations shown in Fig. 2. At this time in the preliminary sequence (Fig. 3f) the runners are at a standstill and the flow is now clearly developed in the reverse direction.

The static pressure is monitored during the simulations at several probe locations. To find how the pressure pulsations change through the sequences, the short-time Fourier transform (STFT) is carried out on the fluctuating component of the pressure. Figure 4 shows spectrograms of STFT from a pressure probe located close to the shroud between the runners. The blade passing frequency (BPF) of each runner, $f_{\mathrm{R1,BPF}}$ and $f_{\mathrm{R2,BPF}}$ for Runner 1 and Runner 2, respectively, indicates a strong power. Harmonic frequencies of the BPFs are also apparent. Furthermore, the linear BPF combination, $f_{\mathrm{R1,BPF}} + f_{\mathrm{R2,BPF}}$, is also visible. In the new sequence (left), the BPFs, harmonics and the linear BPF combination, are showing a strong power up until about 2.8 s. After this point, the whole frequency spectrum indicates a strong power, and the previously dominating frequencies are no longer distinguishable. This wide range of excited frequencies occurs as the load fluctuations on the runners suddenly increase and the flow rate approaches zero as the valve is closing. An explanation for this wide range of excited frequencies is that the runners are mainly mixing the flow as the valve is closed. This mixing generates flow structures in a wide range of scales, as shown in Fig. 3e, which consequently produces pressure pulsations

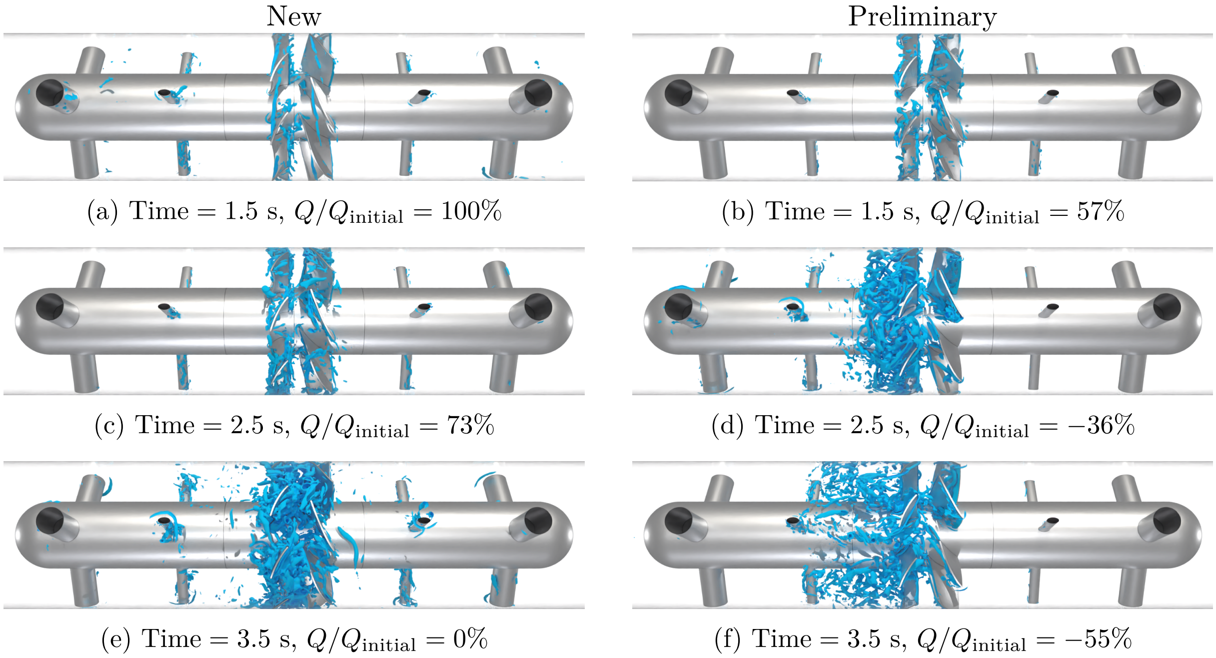

(a) Time = 1.5 s, $Q/Q_{\mathrm{initial}} = 100\%$
(b) Time = 1.5 s, $Q/Q_{\mathrm{initial}} = 57\%$
(c) Time = 2.5 s, $Q/Q_{\mathrm{initial}} = 73\%$
(d) Time = 2.5 s, $Q/Q_{\mathrm{initial}} = -36\%$
(e) Time = 3.5 s, $Q/Q_{\mathrm{initial}} = 0\%$
(f) Time = 3.5 s, $Q/Q_{\mathrm{initial}} = -55\%$

Figure 3. Iso-surfaces of $\lambda_2 = 5 \times 10^5$ s^{-2} at a number of time steps. The preferred flow direction in pump mode is from left to right.

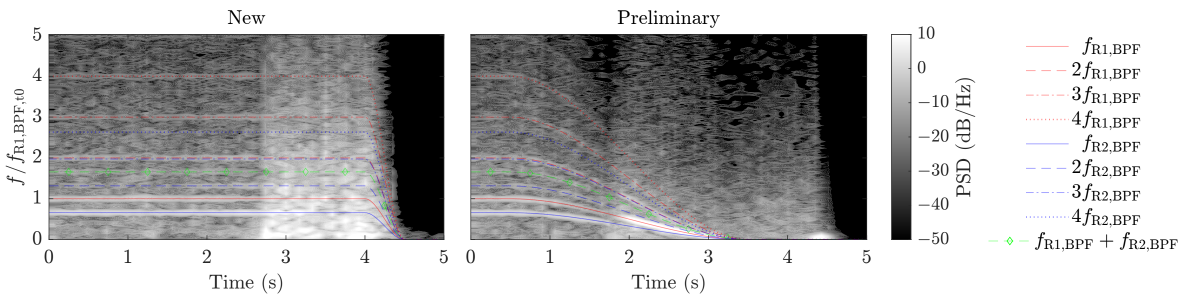

Figure 4. Spectrogram of STFT of the fluctuating pressure component from a probe located at the shroud between the runners. The frequency is normalised by the Runner 1 blade passing frequency at the initial time step, $f_{\mathrm{R1,BPF,t0}} = 150.6$ Hz.

in a broad spectrum. As the rotational speed of the runners is reduced, after 4 s, the power of all frequencies fades away. In the preliminary sequence, a different behaviour is noted. Because the runners are first brought to a standstill, the BPFs, harmonics, and linear BPF combination, are following the reducing rotational speed of the runners. It is seen that the Runner 1 BPF is increasing in power as the flow rate starts to flow in the reverse direction at 1.9 s. Finally, as the valve is closing, some low frequencies are seen at 4.5 s, which occurs as the flow rate is rapidly reduced in the reverse direction. Note that in the preliminary sequence, no such wide range of frequencies is excited as in the new sequence. By only looking at the frequency spectrums in Fig. 4, it is suggested that the preliminary sequence is, in fact, a preferable alternative since the wide range of frequencies is avoided. If the machine is to be shut down several times a day, perhaps it is reasonable to try avoiding the wide range of pressure oscillations that the new sequence produces. The optimal shutdown sequence for the CRPT machine is most likely a trade-off between the valve closing and the speed-down of the runners.

4. Conclusions

Two pump mode shutdown sequences for a contra-rotating pump-turbine have been investigated with computational fluid dynamics simulations in this study. The shutdown sequences are denoted 'preliminary' and 'new' and the main difference is whether a valve closes first or if the runners are brought to standstill first. In the preliminary sequence, the runners are initially brought to standstill, followed by a valve closure. In the new sequence, the opposite is occurring, i.e. a valve closure followed by the speed-down of the runners. It has been shown that the new sequence prevents reverse flow, and compared to the preliminary sequence presents smoother overall load variations. In the preliminary sequence, reverse flow is encountered because the runners are brought to standstill before the valve is closed. As the flow changes its direction, the runner facing the lower reservoir undergoes large load gradients. The torque of that runner is for instance more than quadrupled in a short time. A frequency analysis of pressure fluctuations revealed that the expected blade passing frequency of each runner and the linear combination of the runners' blade passing frequencies are significant through most of the sequences. Furthermore, a wide range of frequencies was excited in the new sequence as the valve was closed while the runners were still rotating. In the preliminary sequence, no such broad spectrum of frequencies where excited. Nonetheless, the new sequence is overall a preferable alternative since reverse flow is avoided and a smoother variation of the main runner loads is generated. However, since the preliminary sequence proposes a more promising frequency spectrum, the optimal shutdown sequence for the contra-rotating pump-turbine is presumably a combination of the two sequences. A suggestion for future studies of the shutdown sequence is to optimise the valve closure in combination with the runners' speed-down to find a trade-off between the new and preliminary sequences.

Acknowledgement

This project has received funding from the European Union's Horizon 2020 research and innovation programme under grant agreement No. 883553. The computations were enabled by resources provided by the National Academic Infrastructure for Supercomputing in Sweden (NAISS) at NSC and C3SE, partially funded by the Swedish Research Council through grant agreement No. 2022-06725.

References

[1] Ansorena Ruiz R *et al.* 2022 *Renewable and Sustainable Energy Reviews* **160** 112281 ISSN 1364-0321
[2] Hoffstaedt J P *et al.* 2022 *Renewable and Sustainable Energy Reviews* **158** 112119 ISSN 1364-0321
[3] 2022 ALPHEUS H2020 URL `https://alpheus-h2020.eu/` accessed on 09 May 2023
[4] Fahlbeck J, Nilsson H and Salehi S 2021 *Energies* **14** 3593 ISSN 1996-1073
[5] Fahlbeck J, Nilsson H and Salehi S 2022 *IOP Conference Series: Earth and Environmental Science* **1079** 012034 ISSN 1755-1315
[6] Fahlbeck J, Nilsson H and Salehi S 2023 *Journal of Energy Storage* **62** 106902 ISSN 2352-152X
[7] Truijen D P K, De Kooning J D M and Stockman K 2021 Drivetrain Architectures for a Mechanically Decoupled Contra-Rotating Reversible Pump-Turbine *2021 IEEE/ASME International Conference on Advanced Intelligent Mechatronics (AIM)* pp 7–12 ISSN 2159-6255
[8] Egorov Y and Menter F 2008 Development and Application of SST-SAS Turbulence Model in the DESIDER Project *Advances in Hybrid RANS-LES Modelling* ed Peng S H and Haase W (Berlin, Heidelberg: Springer) pp 261–270 ISBN 978-3-540-77815-8
[9] Sotoudeh N, Maddahian R and Cervantes M J 2020 *Renewable Energy* **151** 238–254 ISSN 0960-1481
[10] Salehi S, Nilsson H, Lillberg E and Edh N 2021 *Renewable Energy* **179** 2322–2347 ISSN 0960-1481
[11] Weller H 2012 *Monthly Weather Review* **140** 3220–3234 ISSN 1520-0493, 0027-0644
[12] Jasak H 1996 *Error analysis and estimation for the finite volume method with applications to fluid flows.* (Imperial College London (University of London))
[13] Aguerre H J, Márquez Damián S, Gimenez J M and Nigro N M 2017 *Journal of Computational Physics* **335** 21–49 ISSN 0021-9991
[14] Fahlbeck J, Nilsson H and Salehi S 2022 *OpenFOAM Journal* **2** 1–12 ISSN 2753-8168